

Investigation of robust flexible conformal THz perfect metamaterial absorber

Ju-Hyung Kim¹ · Mohammad P. Hokmabadi¹ · Soner Balci¹ · Elmer Rivera¹ · David Wilbert¹ · Patrick Kung¹ · Seongsin Margaret Kim¹

Received: 21 August 2015 / Accepted: 10 November 2015 / Published online: 14 March 2016
© Springer-Verlag Berlin Heidelberg 2016

Abstract The flexible metamaterials have promised to greatly expand our ability to realize a wide range of novel applications including new methods of sensing and cloaking. In this work, flexible metamaterial absorbers, targeted to operate at terahertz frequencies, have been designed, simulated, and fabricated. The absorber structure consisted of a conducting ground plane, a dielectric spacer, and a frequency selective surface which was composed of two layers of nonconcentric, differently sized, single-ring arrays. Absorber structure was designed and simulated such that absorbers exhibited two distinct resonance frequencies with the strength of absorption for both sensitive to the center-to-center spacing of the rings and polarization. The functionality of the absorbers was seen to be similar both in planar and deformed positions, which promises robustness of the conformal flexible metamaterials device under the deformation and uneven surfaces.

1 Introduction

The terahertz (THz) spectral region remains a scientifically rich but yet technologically underdeveloped research area. Nevertheless, THz frequencies attract great attention due to their potential applications, including biomedical imaging [1, 2], materials characterization [3, 4], detection of explosives [5], and astronomy [6]. An unfortunate hurdle is the difficulty in efficiently generating, detecting, and controlling the propagation of radiation at THz frequencies.

Metamaterials hold great promise of improving our ability to manipulate THz radiation. Metamaterials typically consist of arrays of subwavelength resonant structures whose size, geometry, and orientation can be selected to allow for exotic optical properties such as a negative permeability or refractive index. Many different metamaterial structures have been proposed [7–10] for applications such as filters [11, 12], modulators [13, 14], optical cloaks [15, 16], and superlenses [17, 18]. Among them, the terahertz metamaterial perfect absorber [19] is well suited to a variety of applications due to its high efficiency operation. In particular, flexible metamaterials offer many benefits, including the ability to be conformed on nonuniform surfaces while maintaining a high degree of functionality, which makes them suitable for a wide variety of sensing applications such as cloaking [20]. Flexible devices can have many advantages over their nonflexible counterparts. They can be much lighter and smaller when space or weight constraints are critical, and are usually much more durable. One especially advantageous benefit of flexible devices is the ability to be conformed for placement in unusual places and orientations which would be a useful characteristic for metamaterials. Flexible metamaterials are typically fabricated by printing or depositing of metal resonant structures onto a flexible substrate or by applying hybrid lithography approaches and their functionality compared in both fixed and flexible forms [20–22]. Various applications of them such as stress/strain sensing or stealth applications have recently been realized [23–25]. A flexible broadband absorber has also been reported that was composed entirely of flexible polydimethylsiloxane (PDMS) with no metallic resonant structures [26]. However, the effects of surface geometry on the functionality of the flexible devices conformed to it have never been fully investigated.

✉ Seongsin Margaret Kim
seongsin@eng.ua.edu

¹ Department of Electrical and Computer Engineering,
University of Alabama, Tuscaloosa, AL 35487, USA

In this work, we demonstrate robust and flexible metamaterial perfect absorber (FMPA) that works for semi-realistic rough (conformal) surface at THz frequency. The FMPA was designed using finite element method, fabricated by standard photolithography, and characterized with terahertz time-domain spectroscopy (THz-TDS). After verifying the thread of connection between the simulation and measurement, we finally focused this measurement on investigating the practical functionality of the FMPA on a variety of designed uneven surfaces. The functionality of the structures in both fixed and flexible forms was investigated as well as effects on the resonant response due to variation of the resonant element geometry. This was accomplished by using the custom designed vacuum sample holders which can pull the flexible absorbers to be conformed to cylindrical, hemispherical, and pyramid surface relief structures.

2 Design and simulation

The FMPAs were designed using common three layer approach consisting of a bottom copper ground plane, a dielectric spacing layer, and top frequency selective surface (FSS) layer that was composed of ring resonators. The FSS unit cell consisted of two differently sized, nonconcentric, out-of-plane, circular rings separated by a 1.7- μm -thick polyimide dielectric layer as shown in Fig. 1. The ring sizes were selected to target resonant frequencies near 0.75 THz. The unit cell structure was designed such that the larger ring was in the upper layer so that the resonance

of both rings could be easily optimized. A series of four arrays with FSS ring center-to-center spacing (the lateral distance between the centers of the top ring and bottom rings indicated by the parameter Lat in Fig. 1) ranging from 2 to 8 μm were simulated at 0° and 90° polarizations to determine the effect of this spacing on the resonant frequencies and absorption strength at each frequency. Table 1 shows the design parameters for the four different structures.

The simulation models were built based on the listed center-to-center displacements. The constructed unit cell was a total of 104 μm square with periodic boundary conditions used to model the FSS array. The nonconcentric nature of the unit cell resulted in a polarization-dependent resonant response in the structures as shown in Fig. 2. For the 0° polarization, the structure developed a single resonant frequency. The frequency was seen to slightly increase from 0.75 to 0.76 THz as the center-to-center displacement of the FSS rings was increased. Each of the rings had a different resonant frequency when the electric field was oriented at 90° , along the long axis of the rings, but the two resonant frequencies were very close together at 0.74 and 0.8 THz. Simulations showed that each ring developed its own strong dipole resonance with the larger ring resonance corresponding to lower frequency at 0.74 THz.

The simulation results for the 90° polarization revealed that the absorbance strength at both resonant frequencies was dependent on the center-to-center displacement. The first resonant frequency at 0.74 THz was seen to decrease from 96 % at the 2 μm displacement before reaching a minimum of 83 % at the 6 μm displacement and finally increasing back to 97 % at 8 μm . The second resonant frequency had opposite behavior starting 71 % and increasing to 94 % at 6 μm before returning to 71 % at 8 μm . These results indicated that the response of the structure to shifting of the unit cell rings could be exploited for sensing applications based on the center-to-center displacement [27].

3 Experimental procedure

The fabrication of the flexible absorbers began with the application and curing of a 10.7- μm -thick layer of polyimide (HD-MicroSystems PI-2610) on a 3" diameter sacrificial Si wafer by spin coating and curing hard bake at 350 $^\circ\text{C}$ for 30 min. This polyimide layer would serve as the flexible substrate. The metal ground plane consisting of a 15 nm Cr adhesion layer and 185 nm Cu layer was deposited onto the polyimide substrate by electron beam evaporation deposition. An additional 10.7- μm -thick layer of polyimide that would make up the dielectric spacer layer was applied to the metal ground plane. Next, a 250-nm-

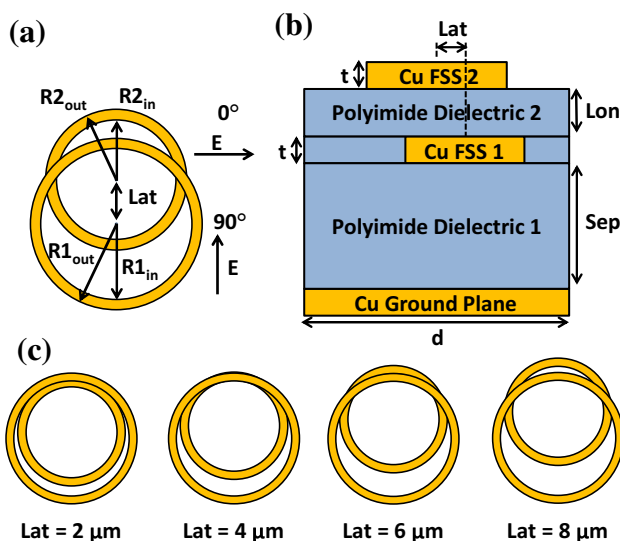


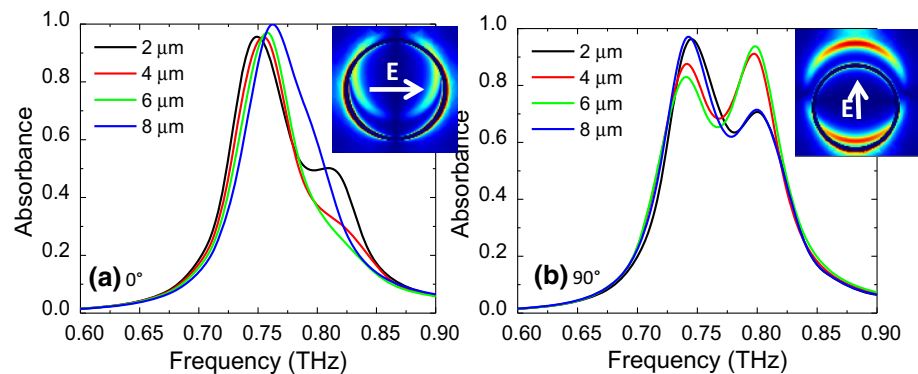
Fig. 1 **a** Top view of the FSS layer consisting of two nonconcentric rings with labeled incident field polarizations, **b** side view, and **c** center-to-center displacement ring geometries of the flexible absorber unit cell

Table 1 First and second rows give the dimensions of the FSS bottom and top rings, respectively

	Structure 1	Structure 2	Structure 3	Structure 4
Bottom ring ($R_{2_{in}}-R_{2_{out}}$)	33–36	33–36	33–36	33–36
Top ring ($R_{1_{in}}-R_{1_{out}}$)	39–42	39–42	39–42	39–42
Displacement (<i>Lat</i>)	2	4	6	8

Third row gives center-to-center displacement (parameter *Lat* in Fig. 1) for each structure

Fig. 2 Simulated absorbance of the FMPAs at **a** 0° and **b** 90° at varied center-to-center ring displacements given



thick SiO_2 layer was deposited which would be the first part of the SiO_2 encapsulation of the first FSS layer. A thin layer of positive photoresist was applied to the SiO_2 by spin coating. The photoresist was then exposed through a dark-field photomask in order to pattern the first FSS layer rings with ion beam etching used to etch the ring patterns to a depth of 200 nm into the SiO_2 . This was followed by E-beam deposition (15 nm Cr/185 nm Cu) of the first FSS layer rings and subsequent lift-off process. The SiO_2 encapsulation was completed with a 50-nm-thick SiO_2 deposition. Then a 1.7- μm -thick layer of polyimide was applied and hard baked to serve as the dielectric spacer between the two FSS layers. Finally, the second FSS layer of rings was patterned by duplicating photolithography process used for the first FSS layer rings, followed by another 15 nm Cr/185 nm Cu E-beam deposition and subsequent lift-off process. The finished flexible absorbers could then be removed from the sacrificial Si wafer. The fabricated structures were inspected by optical microscope between fabrication steps as well as after completion to evaluate FSS ring uniformity. Figure 3a shows an optical microscope image of a fabricated FMPA corresponding to 6 μm center-to-center displacement.

Characterization of the fabricated structures by reflection mode THz-TDS was performed both before and after removal of the flexible absorbers from the sacrificial Si wafer. A photoconductive antenna emitter pumped with a 775 nm ultrafast (120 fs pulsewidth, 76 MHz repetition rate) laser was used with electro-optic sampling detection

in the THz-TDS system. A three-dimensional motion controlled stage was used to position the flexible absorbers in the terahertz beam path. Measurement of the response of the structures to deformation required a unique method for deforming the absorbers. This was accomplished through the use of custom designed vacuum holders that had a recessed region, shown in Fig. 3d, which could be evacuated when covered by the flexible absorbers. The area in this recessed region was populated with an array of surface relief structures in the form of half cylinders or hemispheres, shown in Fig. 3b, c, respectively, to which the flexible absorber would conform under the vacuum. The vacuum sample holders were produced using 3D printing in house.

4 Results and discussion

Analysis of this device has been done based on multiple criteria such as resonant frequency, absorbance at targeted frequency in accordance with the surface shape, and the orientation of different polarization angle of the electric field to make this measurement unique. First of all, the result measured from the fixed device on the flat Si surface, before separating the flexible film from the parental wafer, showed the similar behavior in terms of absorption strengths and resonance frequency changes depending on the displacement of the rings as shown in the Fig. 4 a, b. Although the resonance frequency of measured one shows

Fig. 3 **a** Optical microscope picture of fabricated FMPA with 8 μm center-to-center displacement. **b** cylindrical and **c** spherical surface relief structures. **d** deformation vacuum holder design with device conformation to the **b** and **c**

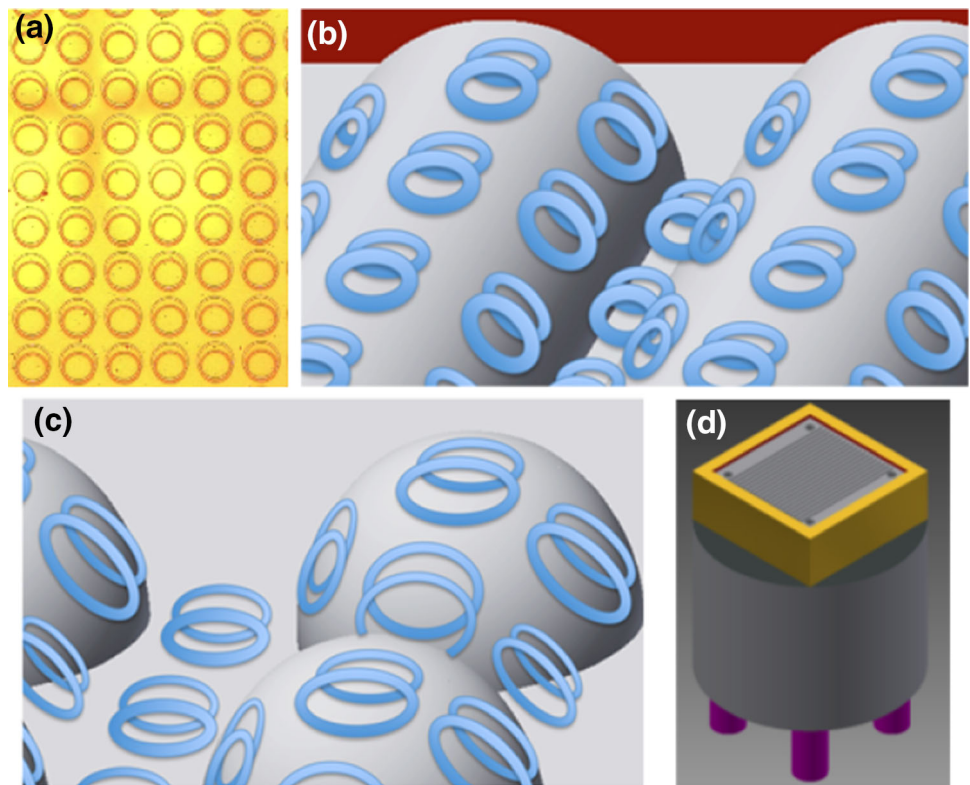


Fig. 4 **a** Simulated and measured absorbance of the FMPAs for fixed one on a parental Si wafer when the center-to-center ring displacements was 6 μm and 8 μm , and **b** measured change in resonant frequency as a function of center-to-center ring displacement at 0° E-field polarization

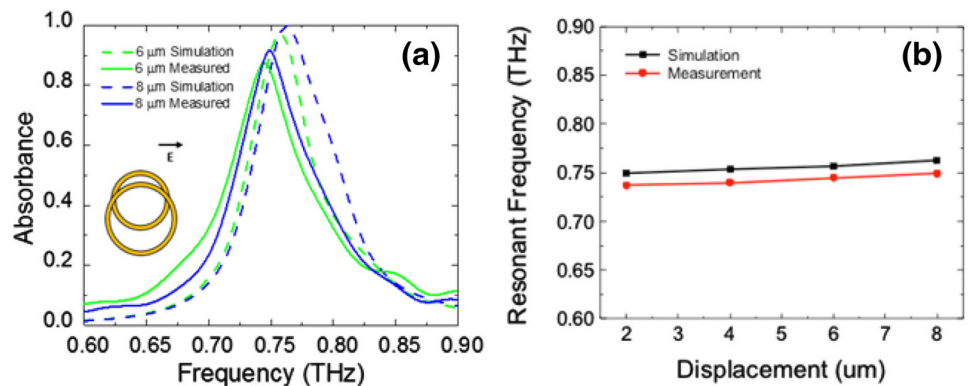
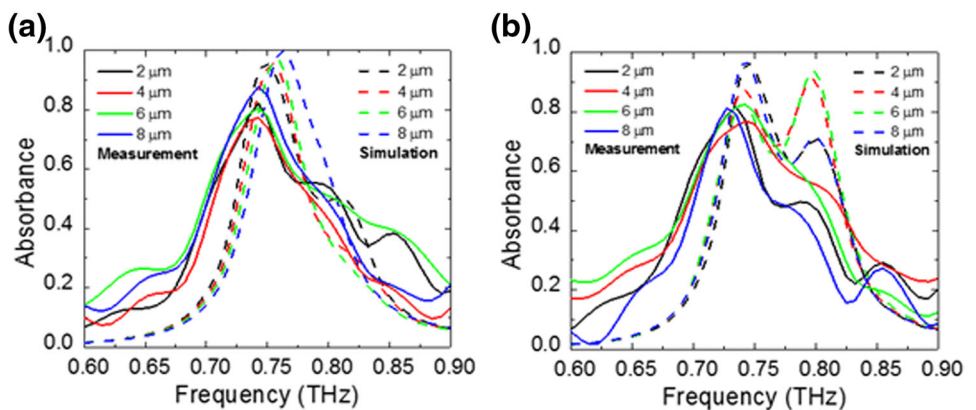


Fig. 5 Measured and simulated absorbance of the FMPAs on a flat surface at **a** 0° and **b** 90° at varied center-to-center ring displacements



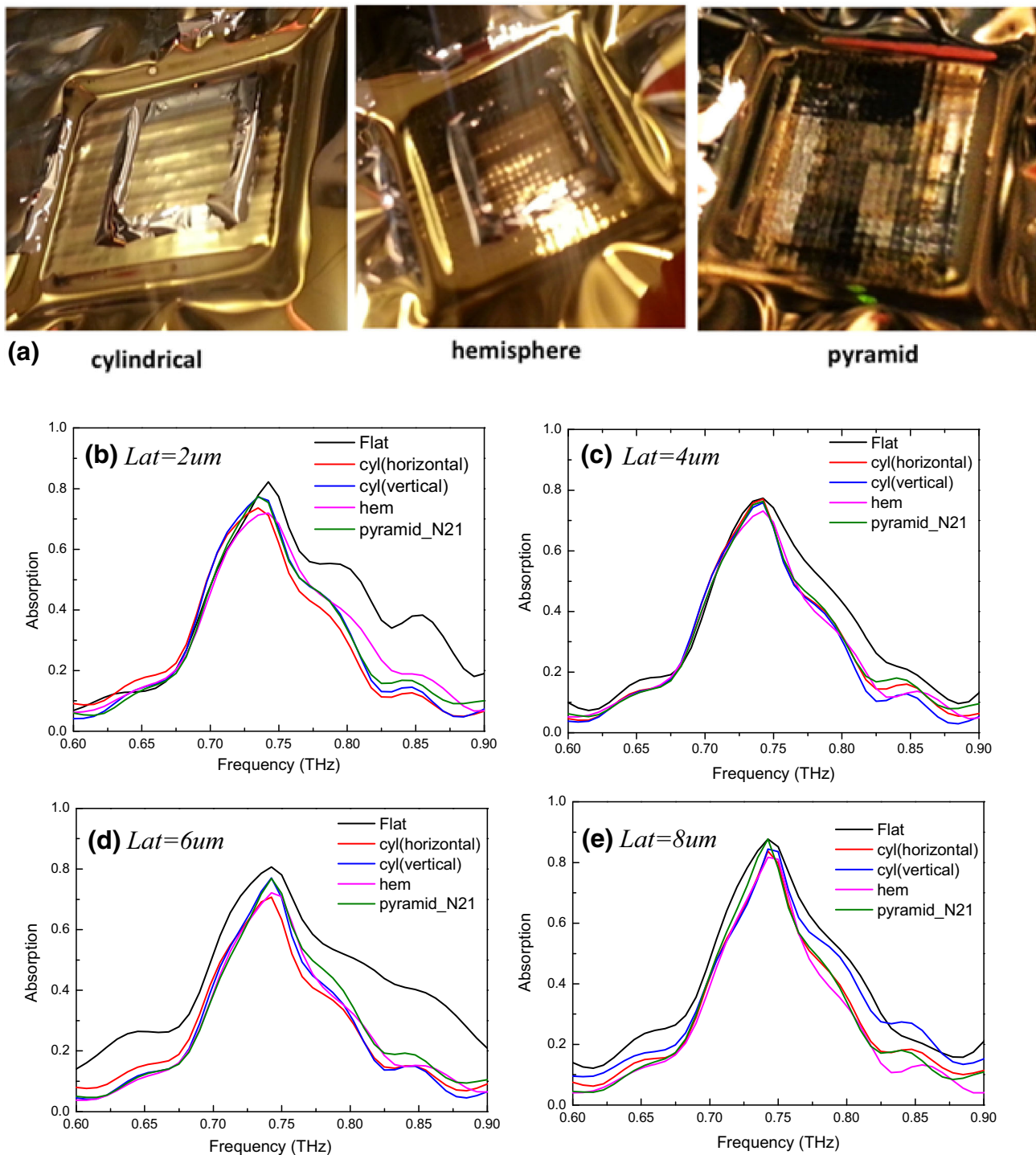


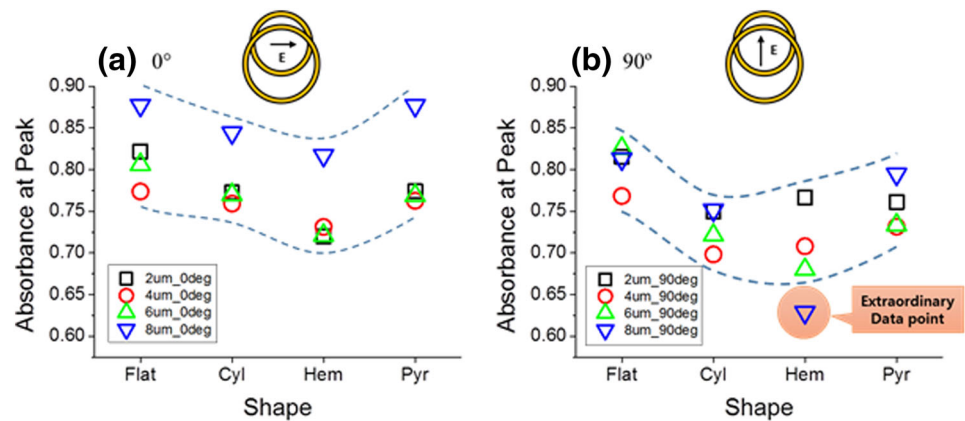
Fig. 6 **a** Optical images of deformed flexible device on *cylindrical*, *hemispherical*, *pyramidal* shape of custom holders by using vacuum force (as indicated). **b–e** Measured absorbance of the FMPA on a various type of surface at 0° E-field polarization with varying displacement distance

approximately 10 GHz lower than the simulation (considering resolution limit is 25 GHz), the performance of a fabricated device was well matched with the simulation.

The measurement of separated device from the Si wafer, which is now flexible but in flat condition also shows kind

of similar results to the simulation as shown in the Fig. 5. The most notable thing in this figure is the existence of second resonance peak around 0.8 THz for both 0° and 90° E-field polarization. For example, in 0° polarization, only $2 \mu\text{m}$ one has second resonance around 0.8 THz in both

Fig. 7 Absorbance at resonant frequency as a function of shape in **a** 0° and **b** 90°



measured and simulated one. In 90° polarization, even though the second resonant peak is not obvious as the simulation of 4 μm and 6 μm one, the absorbance of 4 μm and 6 μm ones is higher than that of the 2 μm and 8 μm ones in both simulation and measurement results. In addition, the shape of absorbance of 2 μm and 8 μm ones are very similar each other. By comparing measurement with simulation, we conclude the device is similarly performing as we expected except undistinguishable second resonant peak at 4 μm and 6 μm displacement in a 90° polarization measurement.

As it is mentioned in the introduction, to verify the robustness of this device with respect to the multiple surface relief structure, the absorbance at the resonant frequency on cylindrical, hemispherical, and pyramidal surface as shown in Fig. 6 had been investigated. To obtain conformity, the flexible device is mounted on the vacuum sample holder where the surface has specific designs. The results from each deformed surface showed the similar trend of resonant peak appearance and shift like observed in the flat surface, within error range of frequency. It is shown in the Fig. 6b–e. In every case, the peak amplitude at the resonant frequency in a flat surface was the highest other than the ones in other deformed surfaces. This was due to the change in orientation of a fraction of the FSS rings during deformation.

For further comparison, we have collected all the peak value of absorbance at the resonant frequency and plotted as a function of shape as shown in Fig. 7.

The most interesting thing is the device which has 8 μm of center-to-center ring displacement had approximately 10 % more absorbance than the other ones in 0° polarization measurement while 8 μm one was not dominant in 90° polarization measurement. In addition, a trend such that higher absorbances of flat and pyramidal surface than the ones of cylindrical and hemispherical surface was identified in both polarization angle. In the meantime, the measured absorption at resonant frequency in 90° polarization

is generally less than the one measured in 0° polarization. However, in general, it still follows the same trend of 0° polarization measurement. As observed, in spite of a little reduction of absorbance in 90° polarization measurement, this result supports the purpose of this measurement such that the device as an absorber carries out its function well in a variety of conformed surfaces.

The robust performance of the designed metamaterial absorber can be explained by the interference theory of perfect metamaterial absorbers [28]. The reflected wave off the FSS gets out of phase with the compounded reflected waves of multiple reflections inside the subwavelength cavity. Therefore, at target frequency the reflection reduces to zero and absorption increases to almost 100 % in theory. This interpretation predicts a large incident angle for metamaterial absorbers without remarkable change in their response. As long as the angle of three-dimensional features on the designed conformal surfaces does not exceed the critical incident angle of the absorber, the response of our flexible metamaterial absorber will remain unchanged.

5 Conclusion

Here we have reported flexible metamaterials perfect absorbers that were designed, simulated, fabricated with photolithography, and characterized by reflection mode terahertz time-domain spectroscopy. The structure consisted of a metal ground plane, a polyimide dielectric spacer, and a FSS composed of two layers of nonconcentric, differently sized, circular ring resonators. We showed by simulation and verified by measurement that the FMPA resonant response is dependent on the center-to-center displacement of the FSS unit cell rings which could be exploited for sensing applications. Additionally, the functionality of the FMPAs in fixed and flexible forms, as well as while under deformation, was evaluated and found to be consistent and robust. This result could lead to future

applications in various cloaking since this FMPA showed enough robustness when it covered other object whose surface is rough and uneven.

Acknowledgments This work was partially supported by the NSF CAREER Award (ECCS-0955160), BRIGE and the NSF Award ECCS-1441947. J. H. K acknowledges Navy Fellowship from South Korea.

References

1. K.F. Ross, R.E. Gordon, Water in malignant tissue, measured by cell refractometry and nuclear magnetic resonance. *J. Microsc.* **128**(1), 7–21 (1982)
2. C.S. Joseph, R. Patel, V.A. Neel, R.H. Giles, A.N. Yaroslavsky, Imaging of ex vivo nonmelanoma skin cancers in the optical and terahertz spectral regions. *J. Biophotonics* **10**(1002), 1–10 (2012)
3. D. Grischkowsky, S. Keiding, M. Van Exter, Ch. Fattinger, Far-infrared time-domain spectroscopy with terahertz beams of dielectrics and semiconductors. *J. Opt. Soc. Am. B* **7**(10), 2006–2015 (1990)
4. L. Duvillaret, F. Garet, J.-L. Coutaz, A reliable method for extraction of material parameters in terahertz time-domain spectroscopy. *IEEE J. Sel. Top. Quantum Electron.* **2**(3), 739–746 (1996)
5. W.R. Tribe, D.A. Newnham, P.F. Taday, M.C. Kemp, Hidden object detection: security applications of terahertz technology. *Proc. SPIE* **5354**, 168–176 (2004)
6. T.G. Phillips, J. Keene, Submillimeter astronomy. *Proc. IEEE* **80**, 1662–1678 (1992)
7. J.B. Pendry, A.J. Holden, D.J. Robbins, W.J. Stewart, Magnetism from conductors and enhanced nonlinear phenomena. *IEEE Trans. Microw. Theory Tech.* **47**(11), 2075–2084 (1999)
8. N. Liu, H. Giessen, Coupling effects in optical metamaterials. *Angew. Chem. Int. Ed.* **49**, 9838–9852 (2010)
9. J. Wang, S. Qu, Z. Xu, J. Zhang, Y. Yang, H. Ma, C. Gu, A candidate three-dimensional GHz left-handed metamaterial composed of coplanar magnetic and electric resonators. *Photonics Nanostruct. Fundam. Appl.* **6**, 183 (2008)
10. V. Crnojevic-Bengin, V. Radonic, B. Jokanovic, Fractal geometries of complementary split-ring resonators. *IEEE Trans. Microw. Theory Tech.* **56**(10), 2312–2321 (2008)
11. F. Martín, F. Falcone, J. Bonache, R. Marqués, M. Sorolla, Miniaturized coplanar waveguide stop band filters based on multiple tuned split ring resonators. *IEEE Microw. Wirel. Compon. Lett.* **13**(12), 511–513 (2003)
12. J. García-García, F. Martín, F. Falcone, J. Bonache, I. Gil, T. Lopetegi, M.A.G. Laso, M. Sorolla, R. Marqués, Spurious pass-band suppression in microstrip coupled line band pass filters by means of split ring resonators. *IEEE Microw. Wirel. Compon. Lett.* **14**(9), 416–418 (2004)
13. H.-T. Chen, S. Palit, T. Tyler, C.M. Bingham, J.M.O. Zide, J.F. O'Hara, D.R. Smith, A.C. Gossard, R.D. Averitt, W.J. Padilla, N.M. Jokerst, A.J. Taylor, Hybrid metamaterials enable fast electrical modulation of freely propagation terahertz waves. *Appl. Phys. Lett.* **93**, 091117 (2008)
14. H.-T. Chen, W.J. Padilla, M.J. Cich, A.K. Azad, R.R. Averitt, A.J. Taylor, A metamaterial solid-state terahertz phase modulator. *Nat. Photonics* **3**, 148–151 (2009)
15. S.A. Cummer, B.-I. Popa, D. Schurig, D.R. Smith, J.B. Pendry, Full-wave simulations of electromagnetic cloaking structures. *Phys. Rev. E* **74**, 036621 (2006)
16. D. Schurig, J.J. Mock, B.J. Justice, S.A. Cummer, J.B. Pendry, A.F. Starr, D.R. Smith, Metamaterial electromagnetic cloak at microwave frequencies. *Science* **314**, 977–980 (2006)
17. N. Fang, X. Zhang, Imaging properties of a metamaterial superlens. *Appl. Phys. Lett.* **82**(2), 161–163 (2003)
18. K. Aydin, I. Bulu, E. Ozbay, Subwavelength resolution with a negative-index metamaterial superlens. *Appl. Phys. Lett.* **90**, 254102 (2007)
19. H. Tao, N.I. Landy, C.M. Bingham, X. Zhang, R.D. Averitt, W.J. Padilla, A metamaterial absorber for terahertz regime: design, fabrication and characterization. *Opt. Express* **16**(10), 7181–7188 (2008)
20. H. Tao, A.C. Strikwerda, K. Fan, C.M. Bingham, W.J. Padilla, X. Zhang, R.D. Averitt, Terahertz metamaterials on free-standing highly-flexible polyimide substrates. *J. Phys. D Appl. Phys.* **41**(23), 232004 (2008)
21. J.G. Kim, N. Takama, B.J. Kim, H. Fujita, Optical-softlithographic technology for patterning on curved surfaces. *J. Microtech. Microeng.* **19**, 055017 (2009)
22. S. Walia, C.M. Shah, P. Gutruf, H. Nili, D.R. Chowdhury, W. Withayachumnankul, M. Bhaskaran, S. Sriram, Flexible metasurfaces and metamaterials: a review of materials and fabrication processes at micro- and nano-scales. *Appl. Phys. Rev.* **2**, 011303 (2015)
23. J. Li, W. Withayachumnankul, S. Chang, D. Abbott, Metamaterial-based strain sensors. *Proceedings of ISSNIP*, vol. 6146571, pp. 30–32 (2011)
24. K. Iwaszczuk, A.C. Strikwerda, K. Fan, X. Zhang, R.D. Averitt, P.U. Jepsen, Flexible metamaterials absorbers for stealth applications at terahertz frequencies. *Opt. Express* **20**(1), 635–643 (2012)
25. R. Alaei, C. Menzel, C. Rockstuhl, F. Lederer, Perfect absorbers on curved surfaces and their potential applications. *Opt. Express* **20**(16), 18370–18376 (2012)
26. D.-H. Kim, D.-S. Kim, S. Hwang, J.-H. Jang, Surface relief structures for a flexible broadband terahertz absorber. *Opt. Express* **20**(15), 16815–16822 (2012)
27. M.P. Hokmabadi, D.S. Wilbert, P. Kung, S.M. Kim, Polarization-dependent, frequency-selective THz stereometamaterial perfect absorber. *Phys. Rev. Appl.* **1**, 044003 (2014)
28. H.T. Chen, Interference theory of metamaterial perfect absorber. *Opt. Express* **20**(7), 7165–7172 (2012)